JGR Space Physics

RESEARCH ARTICLE
10.1029/2019JA027710

Statistical Study of Magnetosheath Jet-Driven Bow Waves

Terry Z. Liu[1,2], Heli Hietala[3,4,5], Vassilis Angelopoulos[5], Yuri Omelchenko[6], Rami Vainio[4], and Ferdinand Plaschke[7]

[1]Cooperative Programs for the Advancement of Earth System Science, University Corporation for Atmospheric Research, Boulder, CO, USA, [2]Geophysical Institute, University of Alaska, Fairbanks, Fairbanks, AK, USA, [3]Department of Physics, Imperial College London, London, UK, [4]Department of Physics and Astronomy, University of Turku, Turku, Finland, [5]Department of Earth, Planetary, and Space Sciences, University of California, Los Angeles, Los Angeles, CA, USA, [6]Space Science Institute, Boulder, CO, USA, [7]Space Research Institute, Austrian Academy of Sciences, Graz, Austria

This article is a companion to Liu et al. (2020), https://doi.org/10.1029/2019JA027709.

Key Points:
- From statistical study, we investigate the formation condition and particle acceleration of magnetosheath jet-driven bow waves
- We show that large Alfven Mach number, solar wind plasma beta, and solar wind dynamic pressure are favorable formation conditions
- Jets with bow waves are associated with higher particle energies than jets without bow waves, indicating that particle acceleration is common

Supporting Information:
- Supporting Information S1

Correspondence to:
T. Z. Liu,
terryliuzixu@ucla.edu

Citation:
Liu, T. Z., Hietala, H., Angelopoulos, V., Omelchenko, Y., Vainio, R., & Plaschke, F. (2020). Statistical study of magnetosheath jet-driven bow waves. *Journal of Geophysical Research: Space Physics*, *125*, e2019JA027710. https://doi.org/10.1029/2019JA027710

Received 5 DEC 2019
Accepted 10 APR 2020
Accepted article online 23 MAY 2020

Abstract When a magnetosheath jet (localized dynamic pressure enhancements) compresses ambient magnetosheath at a (relative) speed faster than the local magnetosonic speed, a bow wave or shock can form ahead of the jet. Such bow waves or shocks were recently observed to accelerate particles, thus contributing to magnetosheath heating and particle acceleration in the extended environment of Earth's bow shock. To further understand the characteristics of jet-driven bow waves, we perform a statistical study to examine which solar wind conditions favor their formation and whether it is common for them to accelerate particles. We identified 364 out of 2,859 (~13%) magnetosheath jets to have a bow wave or shock ahead of them with Mach number typically larger than 1.1. We show that large solar wind plasma beta, weak interplanetary magnetic field (IMF) strength, large solar wind Alfvén Mach number, and strong solar wind dynamic pressure present favorable conditions for their formation. We also show that magnetosheath jets with bow waves or shocks are more frequently associated with higher maximum ion and electron energies than those without them, confirming that it is common for these structures to accelerate particles. In particular, magnetosheath jets with bow waves have electron energy flux enhanced on average by a factor of 2 compared to both those without bow waves and the ambient magnetosheath. Our study implies that magnetosheath jets can contribute to shock acceleration of particles especially for high Mach number shocks. Therefore, shock models should be generalized to include magnetosheath jets and concomitant particle acceleration.

1. Introduction

In the magnetosheath, localized fast jets with spatial scales ~1 R_E are often observed (e.g., Plaschke et al., 2018, and references therein). Such magnetosheath jets are characterized by very large dynamic pressure that are comparable to that of the solar wind. Magnetosheath jets are more likely to occur downstream of the quasi-parallel rather than the quasi-perpendicular bow shock (e.g., Plaschke et al., 2013; Vuorinen et al., 2019). One possible reason is that the surface of the quasi-parallel bow shock is rippled (e.g., Gingell et al., 2017; Hao et al., 2017; Karimabadi et al., 2014). If the solar wind crosses the bow shock where the surface is locally tilted, the downstream flow will be less thermalized and decelerated, thus forming a magnetosheath jet that is colder and faster than the ambient magnetosheath flow (e.g., Hietala et al., 2009; Hietala & Plaschke, 2013). Sometimes, solar wind discontinuities (Archer et al., 2012) and foreshock transients (Archer et al., 2014; Omidi et al., 2016) also form magnetosheath jets.

Due to their large dynamic pressure, magnetosheath jets can disturb the magnetopause causing global perturbations in the magnetosphere-ionosphere system. Hietala et al. (2018) observed that magnetosheath jets can compress the magnetopause and trigger dayside magnetic reconnection. Archer et al. (2019) observed that magnetosheath jets can excite eigenmodes of the magnetopause surface. Such perturbations of the magnetopause can result in compressional low-frequency waves in the magnetosphere, localized flow enhancements in the ionosphere, and auroral brightening (e.g., Archer et al., 2013; Hietala et al., 2012; Wang et al., 2018). Because magnetosheath jets are very common (several occurrences per hour), their geospace effect could be quite significant (Plaschke et al., 2016).

When magnetosheath jets are fast enough, they can drive a bow wave or even a shock. Using Cluster observations, Hietala et al. (2009, 2012) observed that when a supermagnetosonic (in the spacecraft frame) magnetosheath jet hit the magnetopause, it formed a secondary shock propagating sunward in the plasma frame. Simulations (e.g., Karimabadi et al., 2014) suggest that when magnetosheath jets compress the ambient plasma, a compressional bow wave or a secondary shock can form ahead of them. Liu, Hietala, et al. (2019) observed such a bow wave driven by a fast magnetosheath jet and demonstrated that the bow wave can accelerate ions to tens of keV. In the paper accompanying this work, Liu et al. (2020) show that the magnetosheath jet-driven bow waves can also accelerate electrons through the shock drift/fast Fermi acceleration.

The particle acceleration by magnetosheath jet-driven bow waves could play an important role in the parent bow shock acceleration. The most widely employed shock acceleration mechanism is diffusive shock acceleration (e.g., Axford et al., 1977; Bell, 1978; Blandford & Ostriker, 1978; Krymsky, 1977; Lee et al., 2012), whereby particles are scattered back and forth between the converging upstream and downstream flow gaining energy through Fermi acceleration. While particles are scattered in the downstream region, magnetosheath jet-driven bow waves/shocks can provide additional acceleration and thus increase the efficiency of diffusive shock acceleration. Therefore, it is necessary to apply a statistical study to further investigate the properties of magnetosheath jet-driven bow waves/shocks such as their favorable solar wind conditions and whether it is common for them to accelerate particles.

In section 2, we will describe how we selected events with the help of an example. In section 3, we will show our statistical results on the favorable solar wind conditions and particle energization. We will conclude and discuss our results in section 4.

2. Data and Methods

We used data from the Time History of Events and Macroscale Interactions during Substorms (THEMIS) mission probes (Angelopoulos, 2008). We analyzed plasma data from the electrostatic analyzer (ESA) (McFadden et al., 2008) and the solid state telescope (SST) (Angelopoulos, 2008) and magnetic field data from the fluxgate magnetometer (Auster et al., 2008). We used OMNI data to infer the solar wind parameters.

We selected magnetosheath jets that have a bow wave or shock by searching the event list reported by Plaschke et al. (2013). As an example, here we use a magnetosheath jet (Figure 1) reported in the accompanying paper (Liu et al., 2020), to help explain how we automatically select events. We define t_0 as the time of the maximum dynamic pressure within magnetosheath jets (vertical solid lines in Figure 1). In order for a magnetosheath jet to supermagnetosonically compress the ambient magnetosheath plasma, the jet should be at least supermagnetosonic in the spacecraft frame. Thus, we calculate the maximum speed V_m during $t_0 \pm 5$ s (yellow region in Figure 1) and require that V_m is larger than the local fast wave speed (averaged within $t_0 \pm 10$ s). In this case, the maximum dynamic pressure is dominated by V_m. Thus t_0 also corresponds to a time when the velocity-based magnetosheath-to-jet transition ends. Because bow waves/shocks have density and field strength enhancements and velocity deflection, we calculate the maximum value of density ρ_m, field strength B_m, and velocity vector $\boldsymbol{V}_m$ during $t_0 \pm 5$ s. We then calculate the average density $\rho_{\rm bg}$, field strength $B_{\rm bg}$, and velocity vector $\boldsymbol{V}_{\rm bg}$ in the background time interval defined as $[t_0 - 120\ {\rm s}, t_0 - 20\ {\rm s}]$ (blue region in Figure 1). We require: $\rho_m/\rho_{\rm bg} > 1.2$; $B_m/B_{\rm bg} > 1.2$; $|\boldsymbol{V}_m - \boldsymbol{V}_{\rm bg}| > 0.4|\boldsymbol{V}_{\rm bg}|$. The reason we chose the background time interval 20 s before t_0 is to ensure that the parameter transition is (relatively) sharp. By applying our criteria, we selected supermagnetosonic magnetosheath jets that have sharp velocity transition with density and field strength enhancements at their leading edge. We then checked each event and removed those surrounded with large amplitude fast-mode fluctuations in the turbulent magnetosheath, in case that such events could just be one of the fluctuations. Finally, we obtained 364 events out of 2,859 (~13%) that have a bow wave/shock.

Some of these bow waves may have steepened into shocks. For the given example event (Figure 1), Liu et al. (2020) calculated the normal, [−0.86, −0.48, 0.08] with uncertainty ~5.8°, using the mixed-mode coplanarity method (Schwartz, 1998) and the normal speed in the spacecraft frame, 521 ± 69 km/s earthward, using conservation of mass flux (Schwartz, 1998). This results in a Mach number of 1.4 ± 0.2. Across the

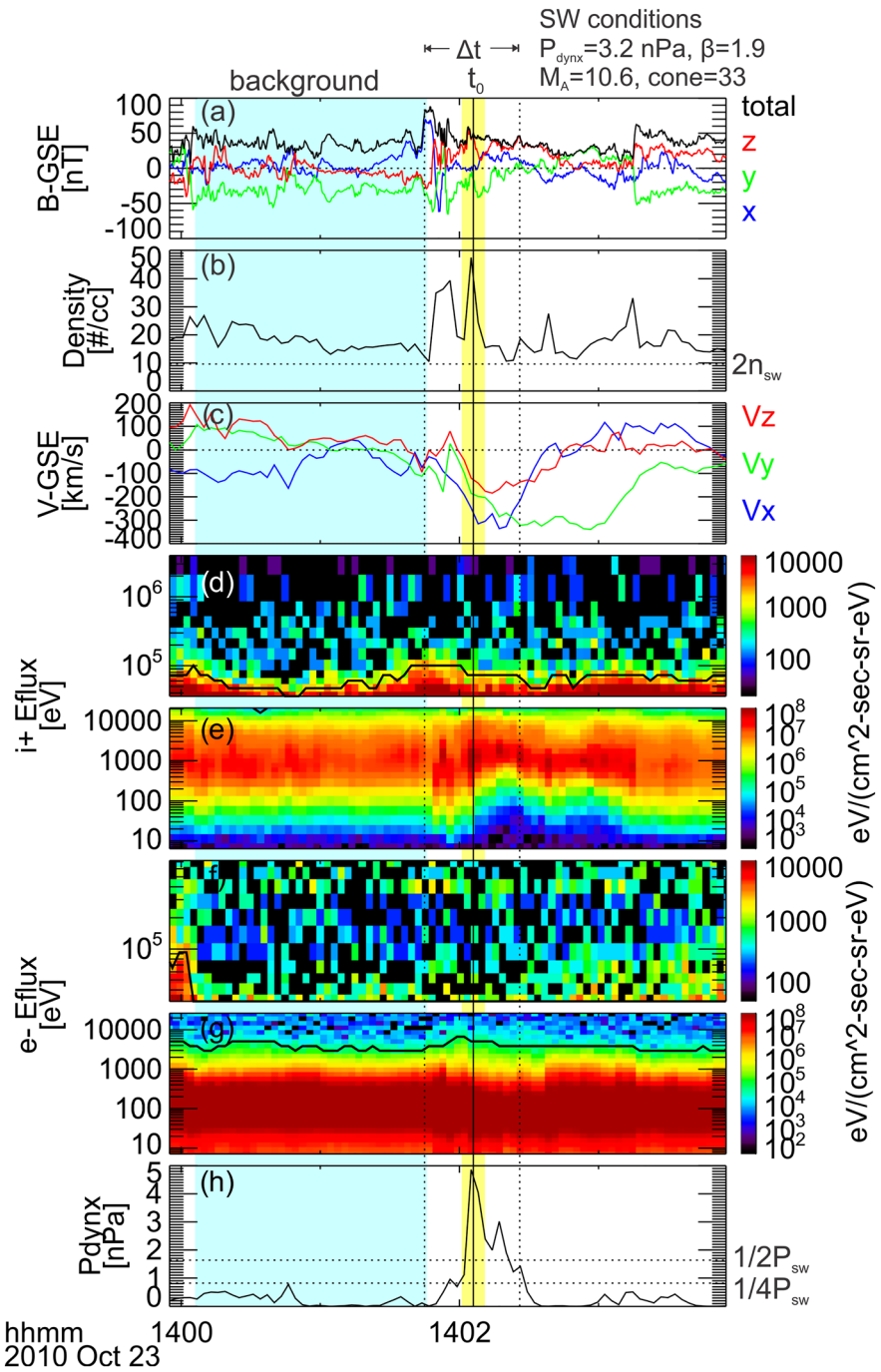

Figure 1. An example of magnetosheath jet-driven shock observed by THEMIS. From top to bottom: (a) magnetic field in GSE (XYZ, total in blue, green, red, and black, respectively); (b) ion density (dotted line indicates 2 times the solar wind density); (c) ion bulk velocity in GSE (XYZ in blue, green, and red, respectively); (d) ion energy flux spectrum from 30 to 700 keV; (e) ion energy flux spectrum from 7 eV to 25 keV; (f) electron energy flux spectrum from 30 to 700 keV; (g) electron energy flux spectrum from 7 eV to 25 keV; (h) dynamic pressure in GSE-X (dotted lines indicate 1/2 and 1/4 of solar wind dynamic pressure, respectively). Black lines in ion and electron spectra indicate the highest-energy channel that have energy flux larger than the instrumental noise level. The blue and yellow regions indicate the time intervals used to calculate the ambient magnetosheath parameters and the jet parameters, respectively.

transition layer, the ion spectrum broadens (Figures 1d and 1e) and the electron energy becomes locally enhanced (Figure 1g), indicating shock heating. Using similar methods, we randomly selected 37 out of 364 events to calculate their shock parameters. Our calculation shows that 36 out of 37 (~97%) events

have Mach number larger than 1 and 34 events (~92%) larger than 1.1 (see Table S1 in the supporting information), indicating that many of them may have steepened or will steepen into shocks. Here we do not distinguish between bow waves and shocks because they could represent the same structure in different stages, and both can accelerate particles.

To determine the statistical characteristics of jet-driven bow waves/shocks, we separated 2,859 magnetosheath jets into two groups, with 2,495 magnetosheath jets without a bow wave/shock (nonshock events) and 364 magnetosheath jets with a bow wave/shock (shock-like events). For each magnetosheath jet the corresponding solar wind parameters are obtained from the OMNI database for time t_0 (averaged over 5 min, which covers the time delay from the bow shock to jets, that is typically 1–2 min; Plaschke et al., 2013). In each group, we calculate the number of events N_i within a certain solar wind parameter range $[\alpha_i, \alpha_i+\Delta\alpha]$. From $P_i = N_i/N$, we obtain the probability distribution as a function of the solar wind parameter, $P(\alpha)$, with a relative error $\sqrt{\left(1-\frac{N_i}{N}\right)/N_i}$, where N = 2,495 or 364. From the time spent by the THEMIS spacecraft in the magnetosheath during the event list (2008–2011; Plaschke et al., 2013), we obtain the amount of time Δt_i when the solar wind parameter is within $[\alpha_i, \alpha_i + \Delta\alpha]$. By calculating $N_i/\Delta t_i$, we thus obtain the number of events per hour in the magnetosheath within $[\alpha_i, \alpha_i + \Delta\alpha]$. Then we can determine whether the occurrence of events depends on the solar wind parameter α. To examine whether such dependencies show differences between the two groups, we also calculate the ratio between their probability distributions and the relative error (the sum of two probability distribution relative errors).

To determine whether there is acceleration/heating associated with magnetosheath jets, we calculate the highest-energy channel that has energy flux larger than the instrumental noise level (black lines in Figures 1d–1g). In the example event, we see that there is moderate increase of the black lines in Figures 1d and 1g, indicating ion and electron energy enhancements around the bow wave. For each magnetosheath jet, we calculate the maximum values of the black lines during $[t_s - 15\ \text{s}, t_0 + 20\ \text{s}]$ (maximum energy), where t_s is the start time of magnetosheath jets when the dynamic pressure exceeds a quarter of the solar wind dynamic pressure (two vertical dotted lines and labeled as Δt in Figure 1). Then we plot the probability distributions of particle energies for the two groups and calculate their ratio to determine whether there are differences.

To further confirm that there is particle acceleration/heating, we compare the ion and electron energy flux around jets with those in the ambient magnetosheath. For each event, we obtain a particle energy spectrum at the time of the maximum energy (maximum value of the black lines in Figures 1d and 1g) during Δt and an averaged spectrum in the ambient magnetosheath during $[t_0 - 400\ \text{s}, t_s - 15\ \text{s}]$. Here we choose a longer time interval than the blue region in Figure 1, because Liu, Hietala, et al. (2019) and Liu et al. (2020) show that the bow wave-accelerated particles can be reflected upstream, adulterating our background energy flux measurements—a longer-interval averaging can reduce this effect. For each event at each energy channel, we obtain averaged background energy flux and the energy flux corresponding to the maximum energy during Δt. At each energy channel, we calculate the value corresponding to the lower quartile (12.5%), median, and upper quartile (87.5%) for the background energy flux and the energy flux of maximum energy and examine whether there are differences between them.

3. Results

3.1. Solar Wind Conditions

Figures 2–4 show the number of events per hour in the magnetosheath as a function of various solar wind parameters. Consistent with a previous statistical study for all magnetosheath jets (Plaschke et al., 2013), nonshock events do not show a dependence on dynamic pressure with maximum occurrence at ~2.5 – 3.0 nPa (Figure 2a). Although shock-like events (Figure 2b) have similar maximum occurrence, they show additional tendency for stronger solar wind dynamic pressure to favor their occurrence. To emphasize this effect, Figure 2c shows the probability distribution ratio of shock-like events to nonshock events. Larger ratios mean that shock-like events are more likely to occur than nonshock ones at a certain solar wind parameter range. We see that these ratios increase with the solar wind dynamic pressure. Thus, larger solar wind dynamic pressure creates a favorable condition for shock-like events.

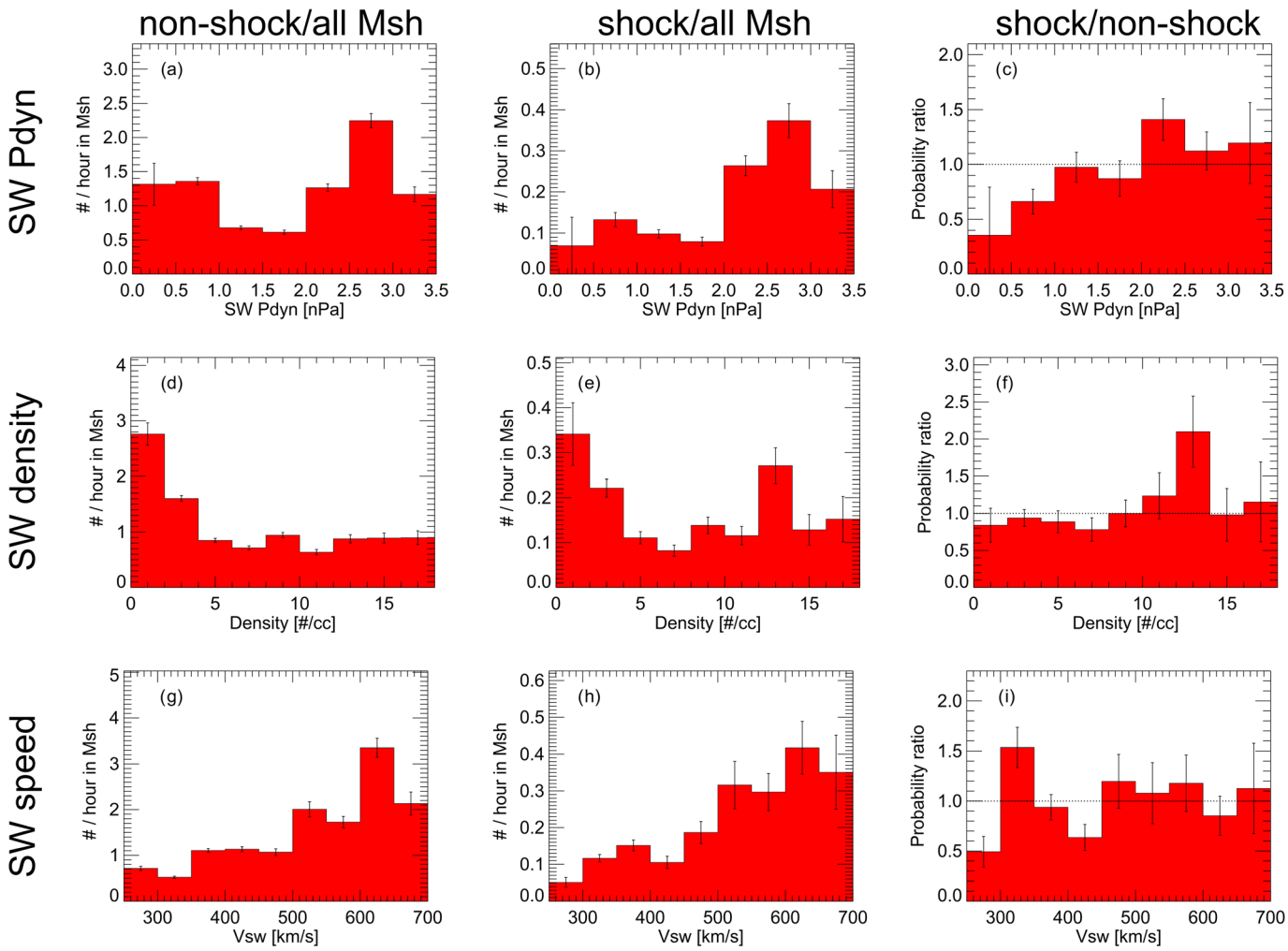

Figure 2. (a) The number of nonshock event per hour in the magnetosheath as a function of the solar wind dynamic pressure. (b) The number of shock-like event per hour in the magnetosheath as a function of the solar wind dynamic pressure. (c) The ratio of shock-like event's probability distribution to nonshock event's probability distribution as a function of the solar wind dynamic pressure. Panels (d)–(f) and (g)–(i) are in the same format as (a)–(c) but as a function of the solar wind density and the solar wind speed, respectively. Bin size is equally distributed. We require the bins shown here cover more than 95% of events in total.

Next, we determine whether this is caused by the solar wind density (Figures 2d–2f) or the solar wind speed (Figures 2g–2i). With regard to the solar wind density, Figures 2d and 2e show similar trends, and their probability distribution ratio does not show clear dependences (Figure 2f). As for the solar wind speed, Figures 2g and 2h are also very similar showing a positive tendency with the solar wind speed, but their probability distribution ratio does not show any dependences either (Figure 2i). Therefore, neither the increased solar wind density nor the increased solar wind speed generates favorable conditions alone.

Next, we look at the solar wind plasma beta (Figures 3a–3c). Figure 3a does not show any trends, but Figure 3b shows a strong tendency for high plasma beta to favor the occurrence of shock-like events. As a result, their probability distribution ratio (Figure 3c) shows a clear trend that the larger solar wind plasma beta has a higher probability to form shock-like events than nonshock events. We then check whether this trend is caused by the solar wind magnetic pressure (Figures 3d–3f) or thermal pressure (Figures 3g–3i). Figure 3f shows a clear trend for shock-like events to occur preferentially at lower magnetic pressure, whereas Figure 3i does not reveal a clear trend with the solar wind thermal pressure. Therefore, the solar wind magnetic pressure seems to be the factor in defining the dependence of shock-like event occurrence on the solar wind plasma beta.

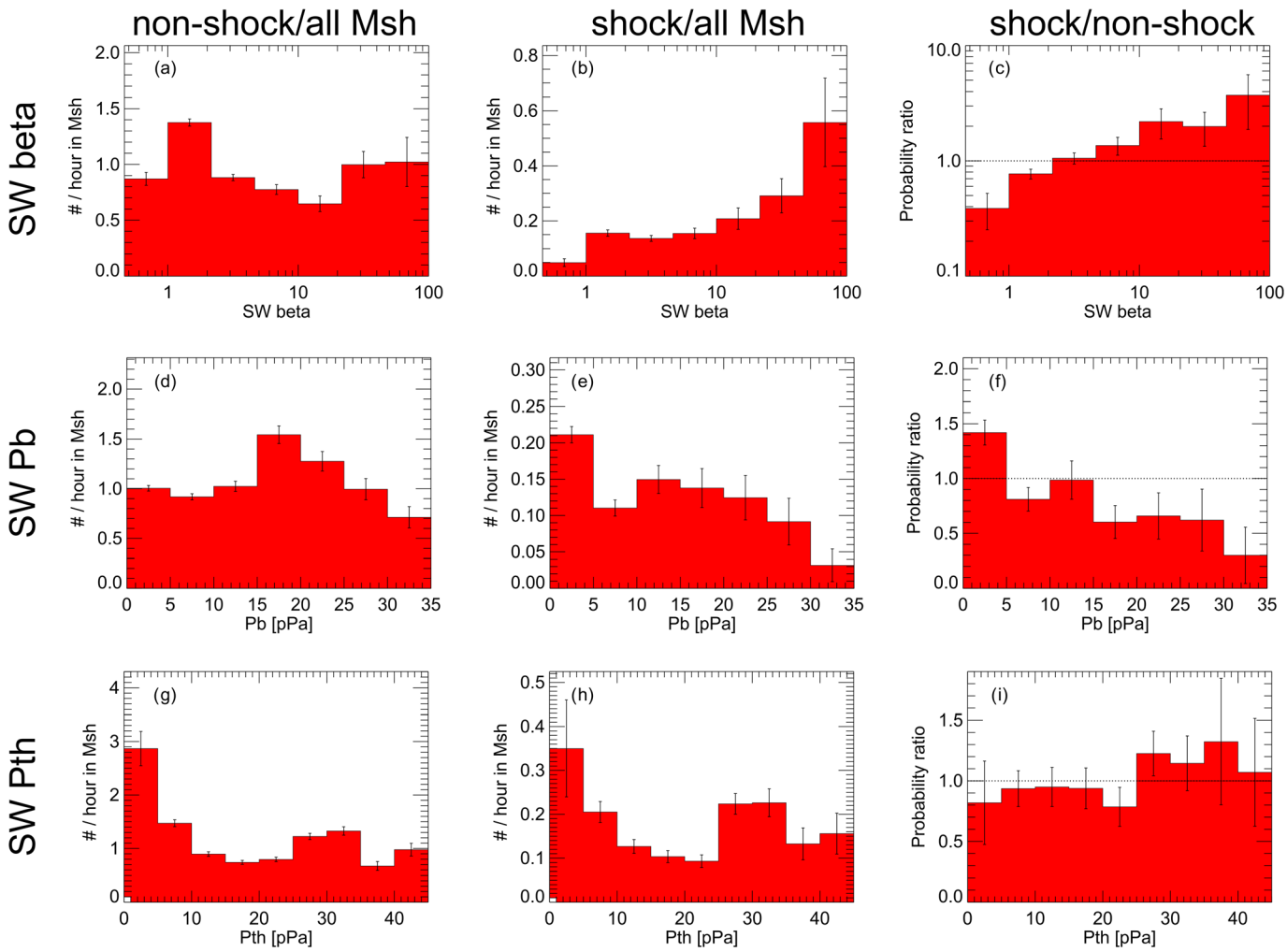

Figure 3. Same format as in Figure 2 but as a function of the solar wind plasma beta (top row), the IMF magnetic pressure (middle row), and the solar wind thermal pressure (bottom row; calculated from beta multiplied by the magnetic pressure).

With regard to the solar wind Alfvén Mach number (Figures 4a–4c), no trends are seen for nonshock events (Figure 4a), whereas the occurrence of shock-like events increases with the Alfvén Mach number (Figure 4b). As a result, their probability distribution ratio clearly increases with Alfvén Mach number (Figure 4c). Note that the ratio of the Alfvén Mach number to the square root of plasma beta is proportional to the ratio of the solar wind speed to the solar wind thermal speed. Since the faster solar wind is hotter (e.g., Elliott et al., 2010), the Alfvén Mach number is proportional to the plasma beta (see Figure S1a). Thus, Figures 3c and 4c are related because of this solar wind speed-temperature correlation. We will discuss how the Alfvén Mach number and plasma beta could affect the formation of shock-like events in section 4.

As for the IMF cone angle, Figures 4d and 4e show negative trends with the IMF cone angle, consistent with the typical property of subsolar magnetosheath jets to occur more frequently during intervals of small cone angle (Plaschke et al., 2013). Their probability distribution ratio also shows weak negative trends (Figure 4f). Thus, smaller IMF cone angles may be a favorable condition for shock-like events. The IMF cone angle could be considered as a proxy for the angle between the IMF and the bow shock normal, θ_{BN}, for subsolar jets. However, it is very difficult to trace the magnetosheath jets backward to the bow shock to calculate local θ_{BN}. Whether the local θ_{BN} plays any role requires more comprehensive studies in the future.

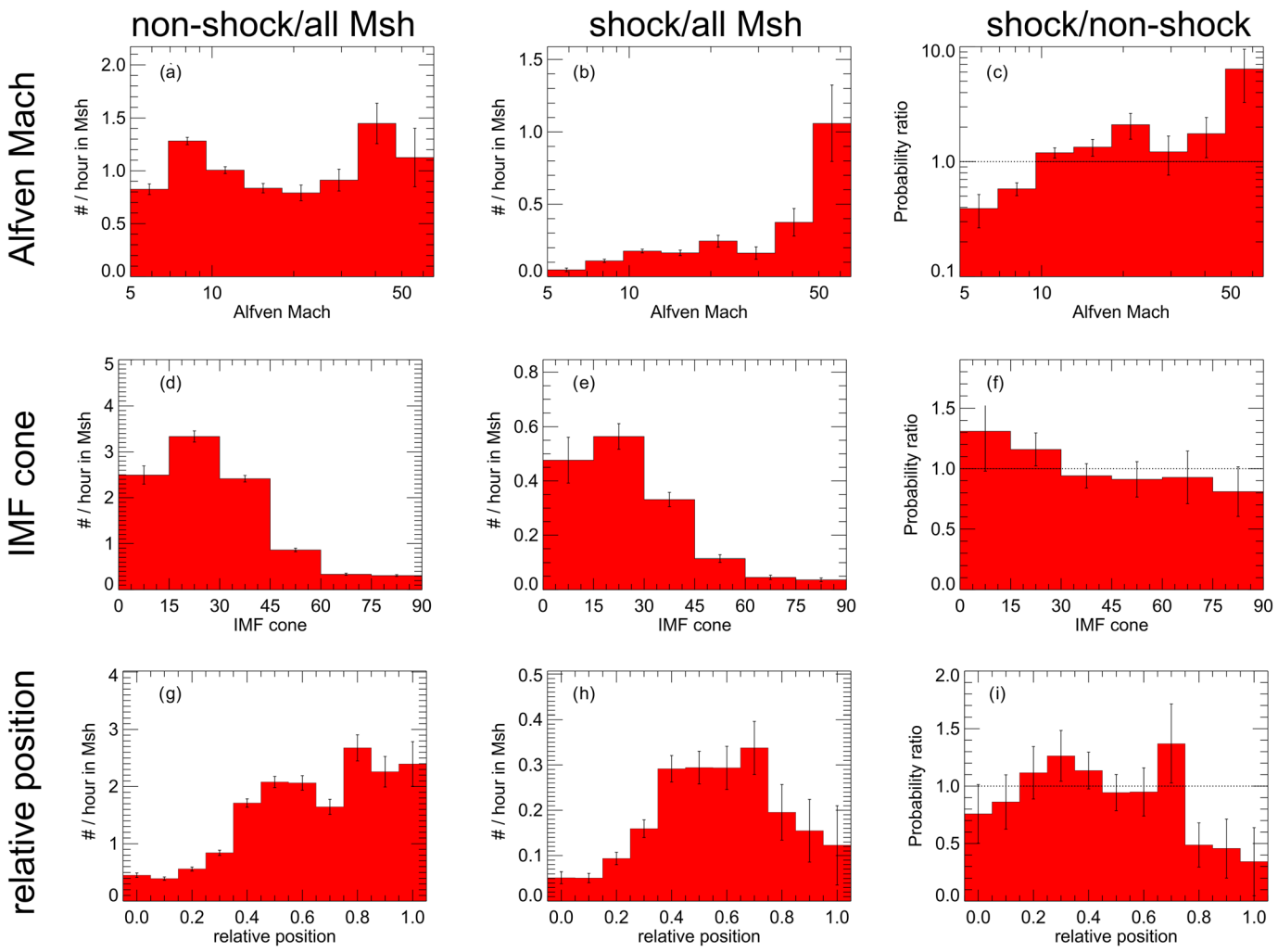

Figure 4. Same format as in Figure 2 but as a function of the solar wind Alfvén Mach number (top row), the IMF cone angle (middle row), and the position relative to the bow shock and magnetopause (bottom row; using Merka et al., 2005 model and Shue et al., 1998 model).

Next, we compare the jets' position relative to the bow shock and the magnetopause (corresponding to 1,0 and 0.0 in Figures 4g–4s), respectively), calculated from the radial distance between the spacecraft position and the model magnetopause (Shue et al., 1998) and normalized by the radial distance between the model bow shock (Merka et al., 2005) and the model magnetopause. Figure 4g shows that there is a higher occurrence of nonshock events closer to the bow shock, consistent with the statistical study by Plaschke et al. (2013). As for shock-like events, Figure 4h shows that for relative positions less than 0.75, the trend is similar to Figure 4g, but for greater than 0.75 (near the bow shock) their occurrence decreases. Therefore, their probability distribution ratio (Figure 4i) shows that shock-like events are much less probable near the bow shock than nonshock events. There are multiple possible explanations. One is that the bow wave/shock needs time to form while the jet propagates away from the bow shock. Another is that deeper in the magnetosheath the flow direction is more along the magnetopause surface, whereas the selection of magnetosheath jets requires that the dynamic pressure in the antisunward direction exceeds half of the solar wind dynamic pressure everywhere in the magnetosheath (Plaschke et al., 2013). As a result, deeper in the magnetosheath the velocity difference between jets and the ambient magnetosheath could be larger than that near the bow shock.

In summary, as expected, the occurrence rates of nonshock events as a function of solar wind parameters are consistent with the previous statistical study for all the magnetosheath jets (Plaschke et al., 2013). However, shock-like events show different properties indicating that larger solar wind plasma beta (due to lower

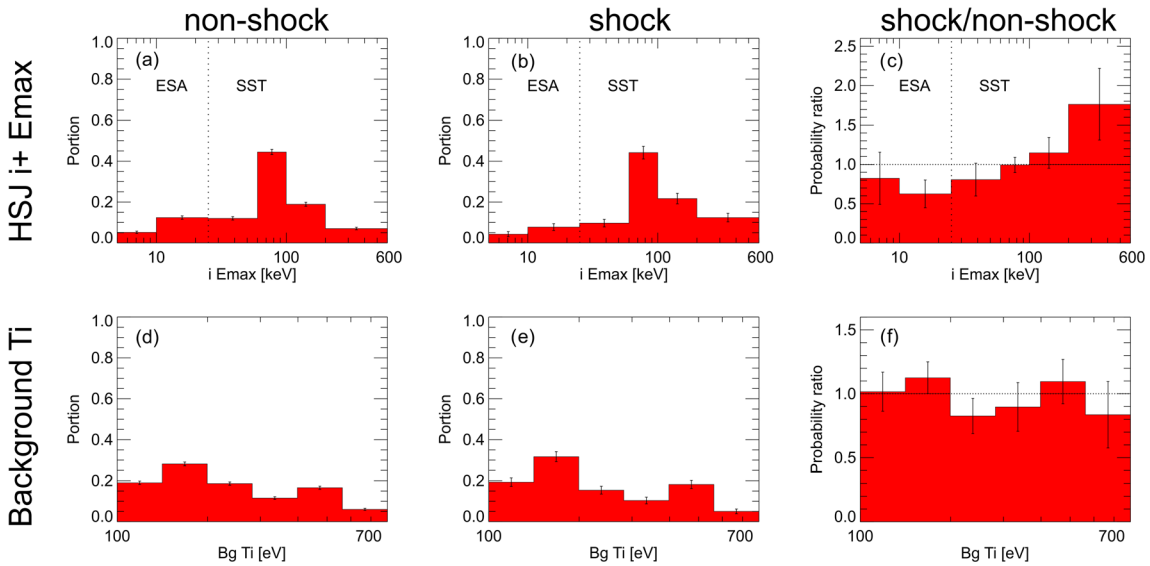

Figure 5. (a) The probability distribution of nonshock events as a function of the maximum ion energy. (b) The probability distribution of shock-like events as a function of maximum ion energy. (c) The ratio of (b) to (a). Panels (d)–(f) are in the same format as (a)–(c) but as a function of background magnetosheath ion temperature. HSJ is short for high speed jet.

magnetic field strength), larger Aflvén Mach number, and larger solar wind dynamic pressure present favorable conditions for their formation. Small IMF cone angles may also play a role. Shock-like events are less likely to occur near the bow shock compared to nonshock events. Hybrid simulations could test these formation conditions in the future.

3.2. Particle Energies

To investigate whether there is particle acceleration/heating associated with jet-driven shocks, we plot the probability distribution of the maximum ion energy and maximum electron energy for the two groups (Figures 5 and 6). We first compare the ion energies. Because 73% (265/364) of shock-like events have SST data (from 30 to 700 keV) available, we only include events that have SST data for both groups (1,619/2495 ~ 65% of nonshock events). From the probability distributions of the maximum ion energy (Figures 5a and 5b), we see that both the nonshock events and shock-like events have the maximum probability at ~60 – 100 keV. This energy range is typical for the magnetosheath ions (e.g., Figure 1d, black line). Above 100 keV, shock-like events have a higher probability than nonshock events. If we calculate the ratio of two probability distributions (Figure 5c), we see more clearly that the shock-like events are more likely associated with higher maximum ion energies than nonshock events.

Before we conclude that this is due to ion acceleration/heating at the magnetosheath jet-driven bow waves/shocks, we need to exclude the possibility that this result is not due to the formation conditions. If shock-like events are biased to occur more often at higher magnetosheath ion temperatures (either due to their formation process or due to the statistical fluctuations in our data set), there will also be higher ion maximum energies associated with shock-like events. We thus plot the probability distributions as a function of the ambient magnetosheath ion temperature (average value in $[t_0 - 120\ \mathrm{s}, t_0 - 20\ \mathrm{s}]$) for the two groups as well as their ratio (Figures 5d–5f). The latter, in Figure 5f, does not reveal any bias. In fact, the magnetosheath ion temperature is proportional to the solar wind speed (see Figure S1b) and we have shown that the solar wind speed does not affect the occurrence of shock-like events. Thus, we confirm that the positive tendency in Figure 5c is not due to the formation conditions but caused by additional acceleration/heating by jet-driven bow waves/shocks.

Next, we compare the electron energies. Only around 50% of shock-like events have electron SST data available. To avoid biases, we plot probability distributions of events with both ESA and SST data and with only ESA data separately. Figures 6a–6c show the probability distributions as a function of the maximum electron energy measured by both ESA and SST. We see that in both ESA and SST energy ranges shock-like events are more likely associated with higher electron energies than nonshock events.

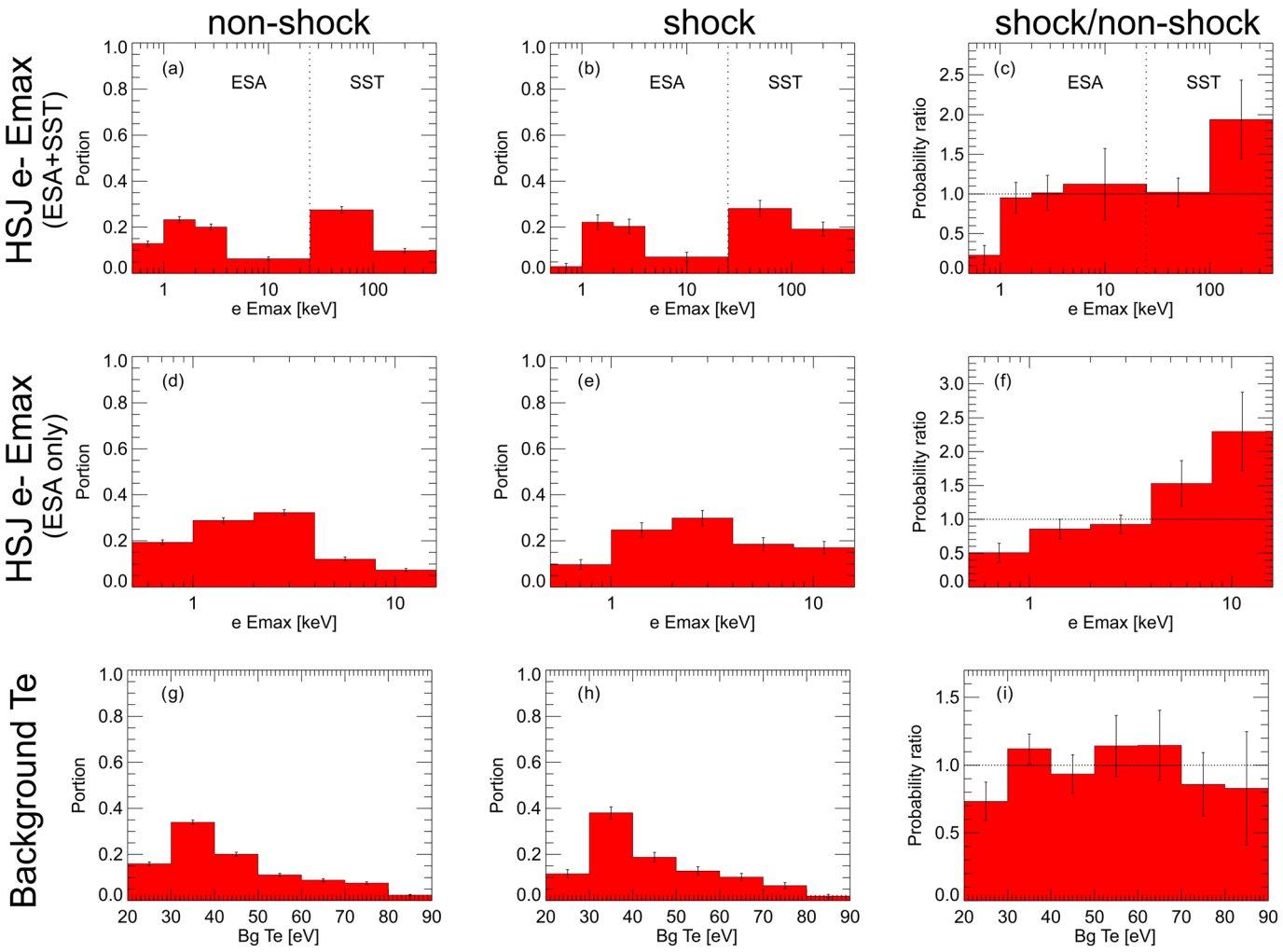

Figure 6. Same format as in Figure 5 but as a function of the maximum electron energy measured by ESA and SST (top row) and by ESA only (middle row), and the background magnetosheath electron temperature (bottom row). Note that because SST is more sensitive than ESA, there are very few events at several highest ESA energy channels (10 to 25 keV). Thus, we use a larger bin there.

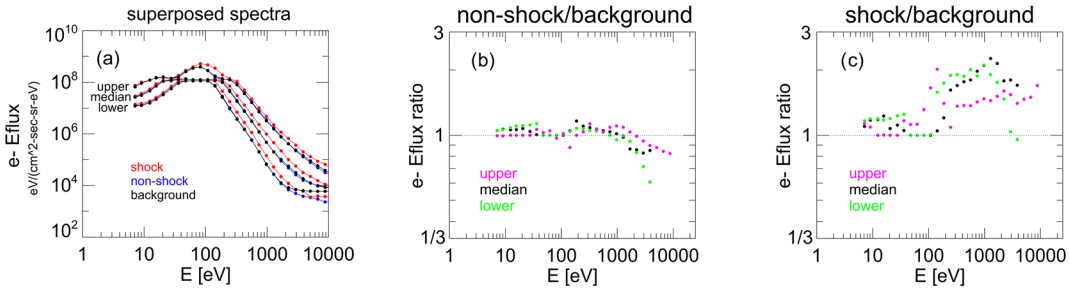

Figure 7. (a) The superposed electron energy flux spectra of shock-like events (red), nonshock events (blue), and the background magnetosheath (black) measured by ESA. Three dots at each energy channel are corresponding to the lower quartile (12.5%), median, and upper quartile (78.5%). Panels (b) and (c) are the ratio of electron energy flux values corresponding to median (black), upper quartile (magenta), and lower quartile (green) of superposed nonshock events to the background magnetosheath and superposed shock-like events to the background magnetosheath, respectively. See text for detail. Note that sometimes electron energy flux measurements saturate at 10^8 eV/(cm^3 · s · sr · eV) in reduced mode.

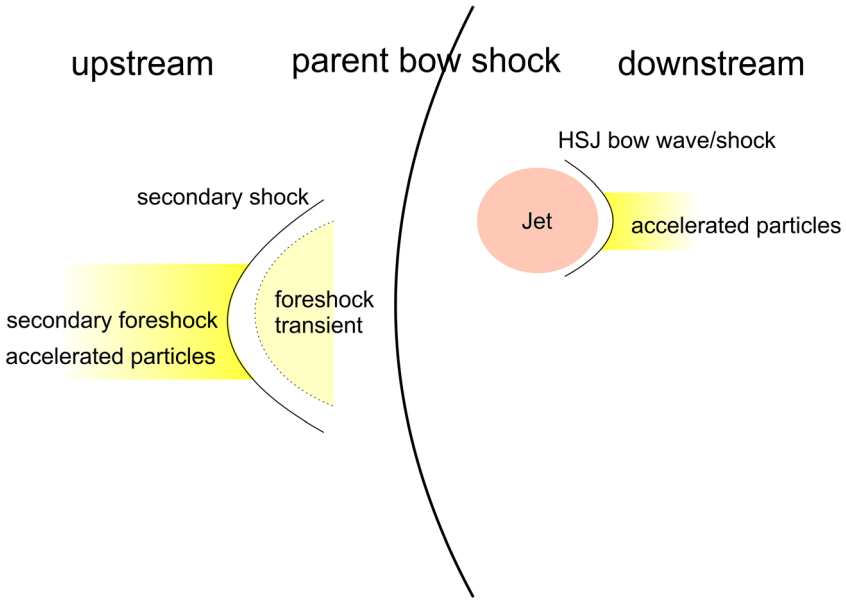

Figure 8. A sketch showing that both upstream and downstream of shocks there are nonlinear structures with a secondary bow wave/shock which can accelerate particles. HSJ is short for high speed jet.

Figures 6d–6f show probability distributions measured only by ESA. There are clear trends that shock-like events have a higher probability to be associated with higher electron energies than nonshock events. Similar to the ions, we also plot the probability distributions of the ambient magnetosheath electron temperature to check for a possible formation condition effect: No preferences for shock-like events are seen (Figures 6g–6i). Thus, our results indicate that shock-like events are more likely associated with electron heating/acceleration than nonshock events.

To further examine whether there are energy increases, we compare the electron energy flux in the background and around the jets. Figure 7a is the superposed electron energy flux spectra (measured by the ESA) of shock-like events (red), nonshock events (blue), and the ambient magnetosheath (black), respectively. We see that the blue lines and black lines almost overlap, but the red lines show larger-energy flux than the blue and black lines above ~100 eV, indicating that shock-like events have enhanced electron energy flux. To see this more clearly, we calculate the ratio of lower-quartile, median, and upper-quartile values between nonshock events and the ambient magnetosheath (Figure 7b) and between shock-like events and the ambient magnetosheath (Figure 7c), respectively. We see that for nonshock events the ratio is ~1 at all energy channels meaning that magnetosheath jets without a bow wave/shock do not change electron energy spectra in the ambient magnetosheath. As for shock-like events, we see that above 100 eV the ratios are ~2. This indicates that when there is a bow wave/shock, magnetosheath jets increase the electron energy flux by a factor of 2 on average at energies above 100 eV. This result is consistent with a multicase study in the accompanying paper (Liu et al., 2020) demonstrating that the bow wave/shock can enhance the electron energy flux at energies above 100 – 200 eV. Our statistical results further confirm that electron acceleration/heating at these energies is common and systematic.

We also find that magnetosheath jets without a bow wave/shock do not show clear ion energy flux increases (Figure S2). However, when there is a bow wave/shock, the ion energy flux increases at energy channels above tens of keV, consistent with Figure 5c. We do not show it here as the ion distributions cannot be simply described by omnidirectional spectra. This is because ions are typically anisotropic, sometimes with multiple components (e.g., Liu, Hietala, et al., 2019), and the ion bulk velocity is comparable to the thermal velocity.

4. Conclusions and Discussion

Case studies by Liu, Hietala, et al. (2019) and Liu et al. (2020) identified that supermagnetosonic jets can drive a bow wave/shock which can accelerate particles. In this statistical study, we determine the

occurrence and favorable solar wind conditions of jet-driven bow waves/shocks and whether their particle acceleration is common: (1) After examining 2,859 supermagnetosonic magnetosheath jets with increases in field strength and density and large velocity deflection at the leading edge, we identified 364 jets (~13%) that have a bow wave/shock ahead of them. (2) By examining probability distributions of various plasma parameters as a function of various solar wind parameters and comparing those among various databases (with/without bow waves or shocks and for the ambient plasma), we conclude that large plasma beta (or low IMF field strength), large Alfvén Mach number, large solar wind dynamic pressure, and likely also small IMF cone angles are favorable solar wind conditions for shock-like events. We also show that shock-like events are less likely to occur near the bow shock, indicating either temporal or spatial requirement of bow wave/shock formation. (3) By comparing the probability distributions of the maximum ion and electron energies, we show that irrespective of the ambient magnetosheath temperature, shock-like events are more likely associated with higher ion energy and electron energy than nonshock events. By comparing electron energy spectra in the ambient magnetosheath and around the jets, we show that shock-like events have higher energy flux (by a factor of 2 on average) above ~100 eV than the background and nonshock events. This indicates that particle acceleration/heating at magnetosheath jet-driven bow waves/shocks is common.

Such particle acceleration/heating at jet-driven bow waves/shocks could contribute to particle acceleration at parent bow shock (Figure 8). Here we estimate their contribution to commonly employed shock acceleration model, diffusive shock acceleration (e.g., Axford et al., 1977; Bell, 1978; Blandford & Ostriker, 1978; Krymsky, 1977; Lee et al., 2012), in the environment of Earth's bow shock. Depending on solar wind conditions, the occurrence rate/encounter rate of jet-driven bow waves/shocks by a stationary spacecraft/particle ranges from ~0.05 to 0.5 per hour as shown in Figures 2–4b, 4e, and 4h (such encounter rate might be underestimated for moving particles as they could have larger cross-sectional area than stationary spacecraft/particles). Based on case studies on ion acceleration by Liu, Hietala, et al. (2019) and electron acceleration in the accompanying paper (Liu et al., 2020), when ions and electrons are reflected by a bow wave, they can gain twice of the de Hoffmann-Teller velocity (typically thousands of km/s) through shock drift acceleration. For bow waves/shocks with magnetic compression ratio of 2 (loss cone angle of 45°), 50% of incoming suprathermal particles can be reflected and accelerated. We estimate that bow waves/shocks can exist at least 1–2 min to accelerate particles. Therefore, the average velocity gained by particles from bow waves/shocks is estimated as ~50% × 1.5 min × (0.05 to 0.5) hr^{-1} × thousands of km/s _x0007E; several to tens of km/s. For diffusive shock acceleration, each time particles bounce across the bow shock, they gain velocity comparable to the velocity difference between the solar wind and magnetosheath (several hundred km/s) (e.g., Drury, 1983). By including jet-driven bow waves/shocks, each time particles enter the magnetosheath, they gain additional several to tens of km/s. In other words, under favorable solar wind conditions (e.g., high Alfvén Mach number and low beta) jet-driven bow waves/shocks can contribute additional 10% acceleration, that is, first-order modification to diffusive shock acceleration model.

Magnetosheath jets, in principle, should also exist in other shock systems. Our statistical study shows that higher Alfvén Mach number can results in more magnetosheath jet-driven bow waves/shocks (Figure 4b). Certain astrophysical shocks ($M_A > 100$; e.g., Treumann, 2009) and other planetary shocks such as Saturn's bow shock ($M_A \sim 20$; e.g., Masters et al., 2016) can have much higher Alfvén Mach numbers than Earth's bow shock ($M_A \sim 3$–10; e.g., Balogh et al., 2005). Therefore, magnetosheath jet-driven bow waves/shocks may be even more common at other space plasma shocks that have stronger M_A and therefore play a more important role there.

Magnetosheath jets are nonlinear structures downstream of shocks. Upstream of shocks, there are also many nonlinear structures called foreshock transients (Eastwood et al., 2005). Foreshock transients that expand fast enough can also form secondary shocks (see sketch in Figure 8). Liu et al. (2016) and Liu, Angelopoulos, et al. (2019) found that such secondary shocks can accelerate ambient solar wind and foreshock particles similar to magnetosheath jet-driven bow waves which accelerate ambient magnetosheath particles (Liu et al., 2020; Liu, Hietala, et al., 2019). A recent statistical study by Liu et al. (2017) also demonstrated that it is common for foreshock transients to accelerate ions and electrons and possibly provide another first-order modification to shock acceleration models. Therefore, nonlinear structures both downstream and upstream of shocks could provide additional acceleration and thus play a role in shock

acceleration by increasing the parent shock acceleration efficiency and providing a seed population for further acceleration. The relevant shock environment comprises not just the shock itself but also numerous surrounding nonlinear structures with secondary bow waves/shocks, which should be included in future generalized shock models.

Here we discuss why shock-like events more likely occur at large solar wind beta, Alfvén Mach number, and solar wind dynamic pressure. The dynamic pressure of magnetosheath jets is proportional to the solar wind dynamic pressure due to the selection criteria/definition (Plaschke et al., 2013). Because the ambient magnetosheath dynamic pressure is also proportional to the solar wind dynamic pressure, higher solar wind dynamic pressure will result in larger dynamic pressure differences between magnetosheath jets and the ambient magnetosheath. A larger dynamic pressure difference means that there is more free kinetic energy to generate bow waves/shocks. Additionally, because the faster solar wind is hotter (e.g., Elliott et al., 2010), both the solar wind beta and Alfvén Mach number are proportional to the ratio of solar wind dynamic pressure to the magnetic pressure. Therefore, larger solar wind beta and Alfvén Mach number mean that there are larger kinetic energies against smaller magnetic pressure, which makes it easier for magnetosheath jets to drive bow waves/shocks. Another possibility is that higher Alfvén Mach number could cause the bow shock surface to be wavier. When the solar wind crosses more inclined portions of the bow shock surface, more kinetic energy remains to drive a bow wave. In the future, more comprehensive studies are needed to examine these possibilities.

One could argue that higher solar wind speed can cause a larger velocity difference between the jets and ambient magnetosheath and therefore should be a favorable condition. However, as the magnetosheath ion temperature is also proportional to the solar wind speed, higher solar wind speed results in larger magnetosheath fast wave speed, making it more difficult for bow waves/shocks to form. These two effects would counter each other, and thus may diminish any dependence of shock-like event occurrence on solar wind speed.

As our selection criteria, we calculate plasma parameters within $t_0 \pm 5$ s, based on the assumption that t_0 is the time where the parameter transition ends. Here we use a very short time interval (corresponding to three data points of plasma measurements), because we want to ensure that the enhancements of magnetic field strength and density occur simultaneously, that is, represent a fast mode compression. Such a short time interval, however, underestimates the maximum field strength and density enhancements (e.g., Figure 1) and possibly overlooks some shock-like events. For example, if we increase the time interval to 14 s, the event list increases by 10%. Additionally, to ensure that the parameter transition ahead of jets is relatively sharp, we calculate the background parameters 20 s before t_0 corresponding to a distance around several thousand km. However, sometimes the time interval of magnetosheath jets lasts several minutes and strong fluctuations inside them can violate the assumption that t_0 corresponds to a time when the parameter transition ends. In other words, some bow waves could be 1 min before t_0 and thus could get excluded because the background parameters are contaminated. For example, 155 events (out of 2,859; 5%) have the jet start time t_s 60 s before t_0. If we could set up better criteria to select shock-like events, statistically significant differences from nonshock events may be even more noticeable.

Acknowledgments

The work at UCLA and SSI was supported by NASA Grant NNX17AI45G. T. Z. L. is supported by the NASA Living With a Star Jack Eddy Postdoctoral Fellowship Program, administered by the Cooperative Programs for the Advancement of Earth System Science (CPAESS). H. H. was supported by the Royal Society University Research Fellowship URF \R1\180671 and the Turku Collegium for Science and Medicine. The work in the University of Turku was performed in the framework of the Finnish Centre of Excellence in Research of Sustainable Space. R. V. acknowledges the financial support of the Academy of Finland (Projects 309939 and 312357).

Data Availability Statement

We thank the THEMIS software team and NASA's Coordinated Data Analysis Web (CDAWeb, http://cdaweb.gsfc.nasa.gov/) for their analysis tools and data access. OMNI data are available at this site (http://cdaweb.gsfc.nasa.gov/). The THEMIS data and THEMIS software (TDAS, a SPEDAS v3.1 plugin, see Angelopoulos et al., 2019) are available at this site (http://themis.ssl.berkeley.edu).

References

Angelopoulos, V. (2008). The THEMIS mission. *Space Science Reviews*, *141*(1-4), 5–34. https://doi.org/10.1007/s11214-008-9336-1

Angelopoulos, V., Cruce, P., Drozdov, A., Grimes, E. W., Hatzigeorgiu, N., King, D. A., et al. (2019). *Space Science Reviews*, *215*(1), 9. https://doi.org/10.1007/s11214-018-0576-4

Archer, M. O., Hietala, H., Hartinger, M. D., Plaschke, F., & Angelopoulos, V. (2019). Direct observations of a surface eigenmode of the dayside magnetopause. *Nature Communications*, *10*(1), 615. https://doi.org/10.1038/s41467-018-08134-5

Archer, M. O., Horbury, T. S., & Eastwood, J. P. (2012). Magnetosheath pressure pulses: Generation downstream of the bow shock from solar wind discontinuities. *Journal of Geophysical Research*, *117*, A05228. https://doi.org/10.1029/2011JA017468

Archer, M. O., Horbury, T. S., Eastwood, J. P., Weygand, J. M., & Yeoman, T. K. (2013). Magnetospheric response to magnetosheath pressure pulses: A low-pass filter effect. *Journal of Geophysical Research: Space Physics*, *118*, 5454–5466. https://doi.org/10.1002/jgra.50519

Archer, M. O., Turner, D. L., Eastwood, J. P., Horbury, T. S., & Schwartz, S. J. (2014). The role of pressure gradients in driving sunward magnetosheath flows and magnetopause motion. *Journal of Geophysical Research: Space Physics*, *119*, 8117–8125. https://doi.org/10.1002/2014JA020342

Auster, H. U., Glassmeier, K. H., Magnes, W., Aydogar, O., Baumjohann, W., Constantinescu, D., et al. (2008). The THEMIS fluxgate magnetometer. *Space Science Reviews*, *141*(1-4), 235–264. https://doi.org/10.1007/s11214-008-9365-9

Axford, W. I., Leer E., & Skadron G. (1977). *The acceleration of cosmic rays by shock waves* (Vol. 11, pp. 132–137). Plovdiv, Bulgaria: Paper presented at International Cosmic Ray Conference, 15th.

Balogh, A., Schwartz, S. J., Bale, S. D., Balikhin, M. A., Burgess, D., Horbury, T. S., et al. (2005). Cluster at the bow shock: Introduction. *Space Science Reviews*, *118*(1-4), 155–160. https://doi.org/10.1007/s11214-005-3826-1

Bell, A. R. (1978). The acceleration of cosmic rays in shock fronts. *Monthly Notices of the Royal Astronomical Society*, *182*(2), 147–156. https://doi.org/10.1093/mnras/182.2.147

Blandford, R. D., & Ostriker, J. P. (1978). Particle acceleration by astrophysical shocks. *The Astrophysical Journal*, *221*, L29. https://doi.org/10.1086/182658

Drury, L. (1983). An introduction to the theory of diffusive shock acceleration of energetic particles in tenuous plasmas. *Reports on Progress in Physics*, *46*(8), 973–1027. https://doi.org/10.1088/0034-4885/46/8/002

Eastwood, J. P., Lucek, E. A., Mazelle, C., Meziane, K., Narita, Y., Pickett, J., & Treumann, R. A. (2005). The foreshock. *Space Science Reviews*, *118*(1-4), 41–94. https://doi.org/10.1007/s11214-005-3824-3

Elliott, H. A., McComas, D. J., Matthaeus, W. H., & Henney, C. J. (2010). Solar wind speed and temperature relationship. *AIP Conference Proceedings*, *1216*, 98–101. https://doi.org/10.1063/1.3395974

Gingell, I., Schwartz, S. J., Burgess, D., Johlander, A., Russell, C. T., Burch, J. L., et al. (2017). MMS observations and hybrid simulations of surface ripples at a marginally quasi-parallel shock. *Journal of Geophysical Research: Space Physics*, *122*, 11,003–11,017. https://doi.org/10.1002/2017JA024538

Hao, Y., Gao, X., Lu, Q., Huang, C., Wang, R., & Wang, S. (2017). Reformation of rippled quasi-parallel shocks: 2-D hybrid simulations. *Journal of Geophysical Research: Space Physics*, *122*, 6385–6396. https://doi.org/10.1002/2017JA024234

Hietala, H., Laitinen, T. V., Andréeová, K., Vainio, R., Vaivads, A., Palmroth, M., et al. (2009). Supermagnetosonic jets behind a collisionless quasiparallel shock. *Physical Review Letters*, *103*(24), 245,001. https://doi.org/10.1103/PhysRevLett.103.245001

Hietala, H., Partamies, N., Laitinen, T. V., Clausen, L. B. N., Facskó, G., Vaivads, A., et al. (2012). Supermagnetosonic subsolar magnetosheath jets and their effects: From the solar wind to the ionospheric convection. *Annales de Geophysique*, *30*(1), 33–48. https://doi.org/10.5194/angeo-30-33-2012

Hietala, H., Phan, T. D., Angelopoulos, V., Oieroset, M., Archer, M. O., Karlsson, T., & Plaschke, F. (2018). In situ observations of a magnetosheath high-speed jet triggering magnetopause reconnection. *Geophysical Research Letters*, *45*, 1732–1740. https://doi.org/10.1002/2017gl076525

Hietala, H., & Plaschke, F. (2013). On the generation of magnetosheath high-speed jets by bow shock ripples. *Journal of Geophysical Research: Space Physics*, *118*, 7237–7245. https://doi.org/10.1002/2013JA019172

Karimabadi, H., Roytershteyn, V., Vu, H. X., Omelchenko, Y. A., Scudder, J., Daughton, W., et al. (2014). The link between shocks, turbulence, and magnetic reconnection in collisionless plasmas. *Physics of Plasmas*, *21*(6), 062308. https://doi.org/10.1063/1.4882875

Krymsky, G. F. (1977). A regular mechanism for the acceleration of charged particles on the front of a shock wave. *DAN SSSR*, *243*, 1306–1308.

Lee, M. A., Mewaldt, R. A., & Giacalone, J. (2012). Shock acceleration of ions in the heliosphere. *Space Science Reviews*, *173*(1-4), 247–281. https://doi.org/10.1007/s11214-012-9932-y

Liu, T. Z., Angelopoulos, V., Hietala, H., & Wilson, L. B. III (2017). Statistical study of particle acceleration in the core of foreshock transients. *Journal of Geophysical Research: Space Physics*, *122*, 7197–7208. https://doi.org/10.1002/2017JA024043

Liu, T. Z., Angelopoulos, V., & Lu, S. (2019). Relativistic electrons generated at Earth's quasi-parallel bow shock. *Science Advances*, *5*(7), eaaw1368. https://doi.org/10.1126/sciadv.aaw1368

Liu, T. Z., Hietala, H., Angelopoulos, V., Omelchenko, Y., Roytershteyn, V., & Vainio, R. (2019). THEMIS observations of particle acceleration by a magnetosheath jet-driven bow wave. *Geophysical Research Letters*, *46*, 7929–7936. https://doi.org/10.1029/2019GL082614

Liu, T. Z., Hietala, H., Angelopoulos, V., Vainio, R., Omelchenko, Y. (2020). Electron acceleration by magnetosheath jet-driven bow waves. *Journal of Geophysical Research: Space Physics*, e2019JA027709. https://doi.org/10.1029/2019JA027709

Liu, T. Z., Hietala, H., Angelopoulos, V., & Turner, D. L. (2016). Observations of a new foreshock region upstream of a foreshock bubble's shock. *Geophysical Research Letters*, *43*, 4708–4715. https://doi.org/10.1002/2016GL068984

Masters, A., Sulaiman, A. H., Sergis, N., Stawarz, L., Fujimoto, M., Coates, A. J., Dougherty, M. K. (2016). Suprathermal electrons at Saturn's bow shock. *The Astrophysical Journal*, *826*(1), 48. https://doi.org/10.3847/0004-637x/826/1/48

McFadden, J. P., Carlson, C. W., Larson, D., Angelopoulos, V., Ludlam, M., Abiad, R., et al. (2008). The THEMIS ESA plasma instrument and in-flight calibration. *Space Science Reviews*, *141*(1-4), 277–302. https://doi.org/10.1007/s11214-008-9440-2

Merka, J., Szabo, A., Slavin, J. A., & Peredo, M. (2005). Three-dimensional position and shape of the bow shock and their variation with upstream Mach numbers and interplanetary magnetic field orientation. *Journal of Geophysical Research*, *110*, A04202. https://doi.org/10.1029/2004JA010944

Omidi, N., Berchem, J., Sibeck, D., & Zhang, H. (2016). Impacts of spontaneous hot flow anomalies on the magnetosheath and magnetopause. *Journal of Geophysical Research: Space Physics*, *121*, 3155–3169. https://doi.org/10.1002/2015JA022170

Plaschke, F., Hietala, H., & Angelopoulos, V. (2013). Anti-sunward high-speed jets in the subsolar magnetosheath. *Annales de Geophysique*, *31*(10), 1877–1889. https://doi.org/10.5194/angeo-31-1877-2013

Plaschke, F., Hietala, H., Angelopoulos, V., & Nakamura, R. (2016). Geoeffective jets impacting the magnetopause are very common. *Journal of Geophysical Research: Space Physics*, *121*, 3240–3253. https://doi.org/10.1002/2016JA022534

Plaschke, F., Hietala, H., Archer, M., Blanco-Cano, X., Kajdič, P., Karlsson, T., et al. (2018). *Space Science Reviews*, *214*(5), 81. https://doi.org/10.1007/s11214-018-0516-3

Schwartz, S. J. (1998). In G. Paschmann, & P. W. Daly (Eds.), *Shock and discontinuity normal, Mach numbers, and related parameters, from analysis methods for multi-spacecraft data* (pp. 249–270). Noordwijk, The Netherlands: Pub. Div. Eur. Space Agency.

Shue, J.-H., Song, P., Russell, C. T., Steinberg, J. T., Chao, J. K., Zastenker, G., et al. (1998). Magnetopause location under extreme solar wind conditions. *Journal of Geophysical Research*, *103*, 17.

Treumann, R. A. (2009). Fundamentals of collisionless shocks for astrophysical application, 1. Non-relativistic shocks. *Astronomy and Astrophysics Review*, *17*(4), 409–535. https://doi.org/10.1007/s00159-009-0024-2

Vuorinen, L., Hietala, H., & Plaschke, F. (2019). Jets in the magnetosheath: IMF control of where they occur. *Annales de Geophysique*, *37*(4), 689–697. https://doi.org/10.5194/angeo-37-689-2019

Wang, B., Nishimura, Y., Hietala, H., Lyons, L., Angelopoulos, V., Plaschke, F., et al. (2018). Impacts of magnetosheath high-speed jets on the magnetosphere and ionosphere measured by optical imaging and satellite observations. *Journal of Geophysical Research: Space Physics*, *123*, 4879–4894. https://doi.org/10.1029/2017JA024954